

## Effects of mechanical activation parameters on the rheological behavior of acid-treated sepiolite

Kemal Bilir<sup>1</sup>, Utku Çağlar<sup>2</sup>

<sup>1</sup> Eskişehir Osmangazi University, Department of Mining Engineering

<sup>2</sup> Kütahya Construction Chemicals

Corresponding author: bilirk@gmail.com (Kemal Bilir)

**Abstract:** This study investigated the effects of mechanical activation parameters on the rheological behaviour of acid-treated sepiolite. Raw sepiolite samples obtained from the Türktaciri region of Sivrihisar were subjected to mechanical activation using a rotor-stator homogenizer with different rotor speeds (12000-24000 rpm) and activation times (30-1320 seconds) to disperse the fiber bundles. The samples were then treated with nitric acid at various molar ratios to remove dolomite impurities. Optimal acid treatment conditions showed that the sepiolite content could be increased from 84.4% to 91.9% using a nitric acid molar ratio sufficient to dissolve 80% of the dolomite present. Flow curve measurements revealed that increasing rotor peripheral speed (7.98–15.95 m/s) and activation time significantly affected the rheological properties. At 24000 rpm and 15.95 m/s peripheral speed, a significant increase in shear stress was observed in the shear rate range of  $10^0$ - $10^3$  s<sup>-1</sup>. The study demonstrated that mechanical activation parameters and acid treatment significantly affect the rheological behaviour of sepiolite suspensions, with the most stable network formation observed at higher peripheral speeds and longer activation times.

**Keywords:** sepiolite, rotor-stator homogenizer, mechanical activation, nitric acid treatment, rheological properties

### 1. Introduction

Sepiolite is a natural clay mineral of magnesium hydrosilicate belonging to the phyllosilicate group. It has a fibrous structure formed by stacking tetrahedral and octahedral oxide layers and channel cavities continuing along the fibres (Rodriguez et al., 1994). Sepiolite has a wide range of uses thanks to its high surface area, fibrous structure, porous structure, crystal morphology, surface activity, formation of stable suspensions with high viscosity at low concentrations, and its sorptive, catalytic, and rheological properties that create technological application areas (Galan, 1996; Zheng et al., 2011; Suarez and Garcia-Romero, 2012).

In addition to its fibrous and needle-like mineral structure, the number of free cations and surface properties significantly affect the rheological behaviour of sepiolite. Sepiolite minerals, composed of needle-shaped bundles of various lengths and thicknesses, do not swell, opening the planes between the plates in water due to their low cation exchange capacity and chain-like structure (DeLima et al., 2017). When fibre bundles are subjected to dispersion in a polar solvent by a mechanical activation method, many particles are liberated from these bundles. These free particles, with other free particles, form a three-dimensional network structure that traps water in the suspension (Simonton et al., 1988; Santaren, 1993). Consequently, the dispersion becomes a viscous structure that resists flow. Continuous and more intensive mechanical mixing (high energy transfer) reduces the size and number of these bundles, causing the number of free particles to increase further and a more complex multiple network to form. This increases the resistance to flow, i.e., viscosity, and water retention capacity (Alvarez, 1984; Çınar, 2005).

Sepiolite bundles that are mechanically activated and liberated in water prevent collapse by supporting each other (Simonton et al., 1988; Santaren, 1993). The network structure is upheld by

various forces between the particles, along with Van der Waals forces and hydrogen bonds connecting the silanol groups. Due to this characteristic, sepiolite is used as a suspension agent. Other particles in suspension, aside from sepiolite, are trapped in the network formed by sepiolite fibres. The large particles other than sepiolite remain suspended due to the strong forces between the particles that maintain the sepiolite network structure.

The liberation and separation of fibre bundles from each other by mechanical activation is only possible by mechanical methods, as it does not occur because of the hydration of displaced interlayer cations as in layered clays. Therefore, the bundles must be activated in polar solvents with special methods to disperse them into free fibres without damaging the fibres. These properties of sepiolite provide great advantages over other clays (Santaren, 1993; Simonton et al., 1988). It is thought that silanol groups play an important role in holding the fibres together, affecting the rheological properties of sepiolite suspensions. It has been determined that fibre lengths and thicknesses affect the rheological properties of sepiolite suspensions, and suspensions prepared with sepiolite with long fibre lengths have higher viscosity values and a stable gel structure (Simonton et al. 1988).

Researchers have used methods such as grinding, dispersing, and mixing to break up the fibre bundles that have contaminants trapped between them and remove the contaminants. These methods have resulted in outcomes, including increased specific surface area, decreased fibre size, thinning of the fibres due to surface erosion, and disruption of the tubular structure (Cornejo and Hermosin, 1988; Myers et al., 1999; Vučelić et al., 2002). A significant amount of dispersion energy is required to produce sepiolite suspensions with high rheological properties, and the type of dispersion mechanism used is critical in this regard. A study by Xu et al. (2011) showed that a high-pressure homogenizer could open sepiolite bundles without damaging their micro-morphological properties and that low-energy activation methods, compared to high-energy size reduction methods, can generate a more effective cutting force.

The purpose of this study was to determine the amount of nitric acid in the molar ratio required to dissolve 80% of dolomite in sepiolite mechanically activated by using a rotor-stator homogenizer, as well as to define its changes in the flow curve of sepiolite suspensions evaluated under different operating parameters of the rotor-stator homogenizer using flow curve measurements.

## 2. Material and methods

### 2.1. Material

The experiments used a brown sepiolite sample supplied by Akmin Madencilik, which operates in the Türktaciri region of Sivrihisar, Türkiye. The sample was prepared for use in the experiments after the following steps.

- Drying for 24 hours at 70 °C in a drying oven
- Crushing the sample below 5 mm with a laboratory-type jaw crusher
- Crushing the sample below 2 mm with a laboratory-type hammer crusher
- Reducing and dividing the sample
- Packaging and coding the samples

The sepiolite sample was characterized using particle size distribution, specific surface area, X-ray diffraction (XRD), and X-ray fluorescence (XRF) methods. Chemical and mineralogical analyses of the samples were conducted in the laboratory of Eskişehir Ceramic Research Institute. The results are given in Tables 1, Table 2, and Fig. 1, respectively.

The particle size distribution of sepiolite was obtained with a Mastersizer 2000 particle size analyzer (Malvern, UK). The particle size distribution of sepiolite is shown in Fig. 2. In the measurements,  $d_{90}$ : 1211  $\mu\text{m}$ ,  $d_{50}$ : 503  $\mu\text{m}$ ,  $d_{10}$ : 19.74  $\mu\text{m}$ , weighted average by volume (VWA): 556  $\mu\text{m}$ , and specific surface area (SSA) was determined as 0.165  $\text{m}^2/\text{g}$ .

### 2.2. Method

Considering the difficulties and disadvantages of mechanical removal of high dolomitic impurities from the sample and the efficiency and capacity of enrichment, the acid treatment method, which is one of the chemical enrichment techniques, is a good option (Çağlar, 2019). In the acid treatment experiments,

Table 1. Chemical analysis of sepiolite sample (Çağlar, 2019)

Chemical Composition	SiO <sub>2</sub>	Al <sub>2</sub> O <sub>3</sub>	Fe <sub>2</sub> O <sub>3</sub>	MgO	CaO	K <sub>2</sub> O	LOI	Total
	%	%	%	%	%	%	%	%
Content	52.78	0.91	0.49	23.75	4.57	0.20	17.30	100

Table 2. Mineralogical analysis of sepiolite sample (Çağlar, 2019)

Mineral Name	Formula	Content (%)
Sepiolite	Mg <sub>4</sub> Si <sub>6</sub> O <sub>15</sub> (OH) <sub>2</sub> +6H <sub>2</sub> O	84.00
Dolomite	CaMg(CO <sub>3</sub> ) <sub>2</sub>	13.50
Other	---	2.50

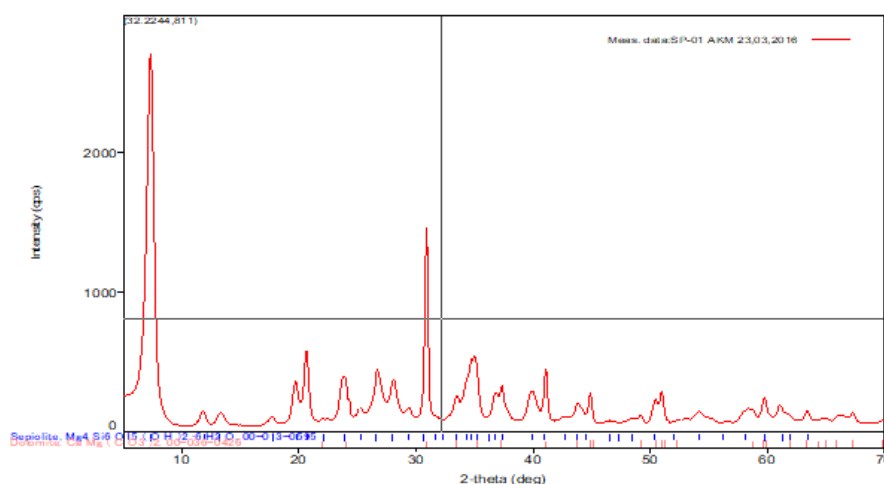


Fig. 1. XRD pattern of sepiolite sample used in this study (Çağlar, 2019)

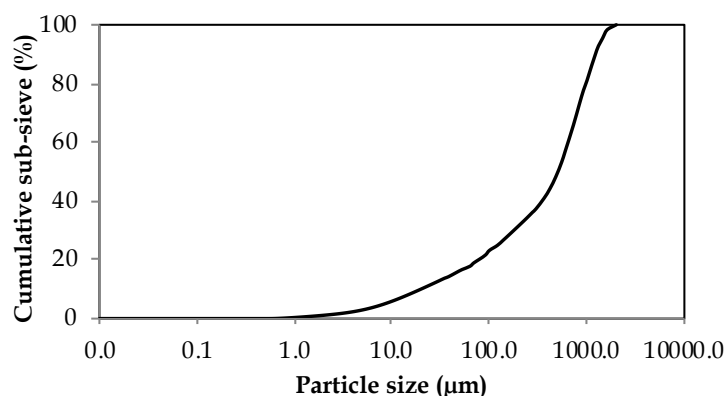


Fig. 2. The particle size distribution of the sepiolite sample (Çağlar, 2019)

nitric acid (HNO<sub>3</sub>) was chosen due to its minimal effect on sepiolite morphology considering the results of previous studies (Jiménez-López et al., 1978; Campelo et al., 1987; Rodriguez et al., 1994; Myriam et al., 1998; Dékány et al., 1999; Çınar et al., 2009; Franco et al., 2014). The mixing period was chosen to be one hour based on preliminary studies. The determined nitric acid concentrations were obtained by mixing the mechanically activated sepiolite suspension with a magnetic stirrer at a stirring speed of 300 rpm, continuously controlling the pH, and gradually adding nitric acid. After 1 hour of mixing, the reaction product was washed with distilled water, dried after neutralizing the pH, and ground with a ceramic mortar to perform XRF chemical and XRD mineralogical analysis. The enrichment efficiency was calculated using the XRF chemical analysis and XRD mineralogical analysis results (Çağlar, 2019).

Although the degree of sepiolite liberation and the fiber size increase the gel stability and viscosity

of sepiolite suspensions, it is also possible that the fiber structure and stability will deteriorate due to high energy-transferred mechanical activation forces. At this point, it was determined that the determination and selection of a system with high shear force and low energy transfer would yield more accurate results. Because of the research conducted, it was determined that rotor-stator homogenizers could be suitable for this process, and the studies were continued within this scope.

The relationship between shear stress and shear rate was evaluated through experimental studies on the rheological characterization of sepiolite. The measurements were correlated with the operating parameters of the applied mechanical activation, and the effects of changes in operating parameters on the rheological properties were investigated. Rheological characterization studies were carried out using the IKA brand T-18 Ultra-Turrax model rotor-stator homogenizer to investigate the operating parameters in a wider shear force range. Table 3 shows the basic parameters of the rotor-stator head design for the homogenizer.

Table 3. Slotted type rotor-stator head design parameters of homogenizer

$D_1 - D_2$	Stator outer & inner diameter, mm	18.95 -13.25
$D - D_3$	Rotor outer & inner diameter, mm	12.70 - 6.89
$d - l$	Stator hole diameter & width, mm	2.10 - 11.48
$W_x - W_y$	Stator blade width & length, mm	2.72 - 8.00
$\delta$	Gap opening, mm	0.2
$S_q$	Number of stator holes, pcs	12
$R_q$	Number of rotor blades, pcs	6
$S_{ha}$	Total area of rotor holes, mm <sup>2</sup>	289
$S_a\%$	Stator open area (Total hole surface area) ratio, %	62
$P_o$	Stator head power number	2.21

The rotor-stator homogenizer's operating parameters were computed using equations 1, 2, and 3, and the rotor-stator mechanical activation parameters were determined (Çağlar 2019).

The "gap" in the rotor-stator homogenizer refers to the clearance between the rotor blades and the stator wall. The shear force created in this region is computed using the equation below.

$$\gamma = \frac{\pi ND}{\delta} \text{ (s}^{-1}\text{)} \quad (1)$$

Here,  $\delta$  is the clearance;  $N$  is the rotor peripheral speed;  $D$  is the rotor outer diameter; and  $\gamma$  represents the cutting forces generated in the clearance.

$$n_{\text{interactions}} = n_{\text{rotor}} * n_{\text{stator}} * N \quad (2)$$

$$E_{\text{rotor}} = P_o * \rho * N^3 * D^5, \text{ (J/s)} \quad (3)$$

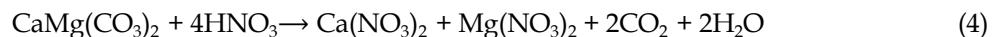
The calculated mechanical activation parameters are nominal shear force ( $N_{sr}$ ), amount of kinetic energy transferred per unit volume (Rotor/volume), and rotor blade-stator hole interaction number (interaction).

Experimental studies were conducted with suspensions prepared at 6% solid concentration in 300 ml volume, 10 cm diameter polyethylene cylindrical sample containers. A 13 ml sample from the suspension was fed to the Bohlin brand CVO 120 model rheometer device. The samples were kept at 25°C before and during the measurement with the Peltier temperature regulation unit connected to the rheometer device. As a result of the preliminary studies, it was determined that the samples reached a rheologically stable state after resting for 10 minutes, and then the measurements were made.

### 3. Results and discussion

#### 3.1. Acid treatment experiments

The enriched solid product obtained after the acid treatment experiments was named "SP-01AKM-X%" in the experiments. The "X" in the name represents 4 times the molar ratio of HNO<sub>3</sub> needed to dissolve one mole of dolomite. This "4" factor was obtained from the chemical reaction equation below.



For example, the expression "SP-01AKM-100%" indicates that the amount of HNO<sub>3</sub> required to dissolve all dolomite in sepiolite was used in the experiment. In contrast, the expression "SP-01AKM-40%" means that the amount of HNO<sub>3</sub> required to dissolve 40% of dolomite in sepiolite was used in the experiment.

The amount of nitric acid required to remove dolomite, the main impurity of sepiolite, was calculated based on Equation (4) and the mineralogical analysis data in Table 2. The results of the experimental study are shown in Tables 4, 5, 6, and 7.

Table 4. Nitric Acid Treatment pH values and Solid Recovery Rates (Çağlar, 2019)

SP-01AKM-X% (X%=)	0%	40%	60%	80%	100%	140%
pH	7.72	7.22	6.91	6.44	5.51	2.45
Solid Recovery Amount (% by weight)	100.00	88.30	84.66	75.75	67.50	33.20

As seen in Table 4, the pH decreases with the increase in acid concentration. Depending on the increasing amount of acid, solid recovery decreases. Given that the dolomite content in SP-01 AKM is 13.5%, it is evident that when mass losses exceed this threshold, sepiolite, undesirable for dissolution in the system, also sustains damage. It is observed that mass losses increase very rapidly when the pH value drops below 6. This situation complies with the sepiolite dissolution diagrams reported in the literature (Tomura et al., 1995; Özdemir and Kıpçak, 2004; Çınar, 2005).

The acid treatment in this study aims to reach the minimum impurity value at the maximum solid concentration. Tables 5 and 6 show the chemical analysis results of the recovered solid and the solution liquid obtained after washing.

Table 5 shows that as the acid concentration increases, the proportion of silicon dioxide increases, while the calcium oxide and magnesium oxide components decrease.

Table 5. XRF analysis results of the recovered concentrated solid (Çağlar, 2019)

SP-01AKM-X% (X%=)	0%	40%	60%	80%	100%	140%
Chemical Content	%					
SiO <sub>2</sub>	52.80	55.68	58.10	60.30	62.29	71.40
Al <sub>2</sub> O <sub>3</sub>	0.91	0.88	0.89	0.90	0.89	0.80
Fe <sub>2</sub> O <sub>3</sub>	0.49	0.50	0.50	0.51	0.50	0.41
MgO	23.75	23.68	23.61	23.43	22.54	17.32
CaO	4.57	2.91	1.53	0.39	0.11	0.03
K <sub>2</sub> O	0.18	0.19	0.19	0.19	0.19	0.11
LOI	17.30	16.17	15.18	14.28	13.49	9.93

Table 6. AAS chemical analysis results of waste solution (Çağlar, 2019)

SP-01AKM-X% (X%=)	0%	40%	60%	80%	100%	140%
Chemical Content	ppm					
Al <sub>2</sub> O <sub>3</sub>	0.15	1.34	1.85	2.44	1.97	92.60
Fe <sub>2</sub> O <sub>3</sub>	0.59	0.59	0.60	0.61	0.69	91.59
MgO	1.79	779.72	1275.70	1826.39	2608.56	12597.36
CaO	2.14	2745.22	4386.48	5088.32	5155.31	5170.98

On the contrary, there is a rapid increase in magnesium and calcium elements in the waste solution (Table 6).

Fig. 3 shows that the acid concentration was higher than the molar ratio needed to dissolve all the dolomite in the mineral. Additionally, the SP-01AKM-140% coded experiment data clearly showed that the silicon oxide ratio went up quickly and the magnesium oxide ratio went down swiftly.

This sudden change is similar to the solid recovery rate. It is interpreted as the dolomite content in the mineral having decreased to a minimum level and the acid molecules having started to damage the sepiolite structure.

It is not feasible to assess the effectiveness of enrichment based solely on solid recovery rates and chemical analysis data. Therefore, quantitative XRD analysis was conducted on the enriched samples (Table 7).

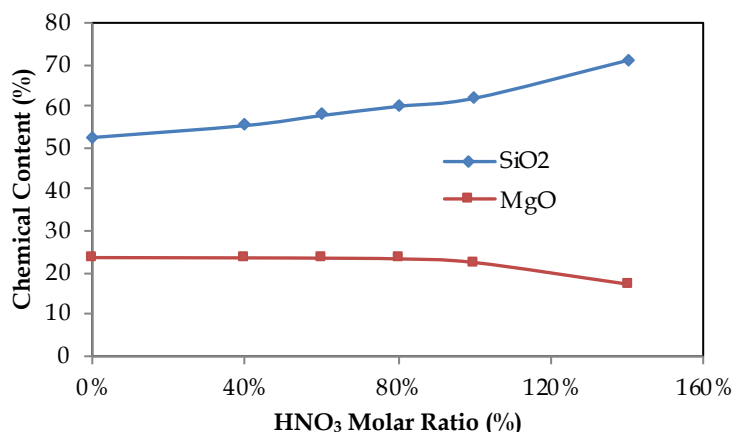


Fig. 3. HNO<sub>3</sub> Molar ratio, magnesium oxide and silicon oxide content change in enriched concentrated solid

Table 7. XRD Mineralogical analysis results of enrichment samples (Çağlar, 2019)

SP-01AKM-X% (X%=)	0%	40%	60%	80%	100%	140%
Mineralogical Content	%					
Dolomite	9.5	5.9	3.0	1.0	0.0	0.0
Sepiolite	84.4	87.7	90.3	91.9	88.3	65.6
Other (Free Silica etc.)	6.1	6.4	6.7	7.5	11.6	34.4
Total	100.0	100.0	100.0	100.0	100.0	100.0

It was found that nitric acid could raise the molar ratio needed to dissolve 80% of the dolomite in sepiolite from 84.4% to 91.9% when the chemical and mineralogical analysis data were evaluated together. When this molar ratio was exceeded, the sepiolite content dropped quickly, reaching 65.6% in the SP-01AKM-140% sample.

As the nitric acid concentration increased from 60% to 80% molar ratio, the dolomite content decreased in parallel, and the free silica content increased along with the sepiolite content (Table 7). When this result was interpreted together with the chemical analysis results, it was determined that from a 60% molar ratio, nitric acid molecules began to damage the structure of sepiolite, and the free silica mineral phase in the pulp began to increase rapidly.

The results of the enrichment yield calculations determining the optimum enrichment conditions where both the solid amount and grade are maximized are given in Table 8.

Table 8. Acid treatment yield after enrichment (Çağlar, 2019)

Sample Name	Concentrate Solid Amount (%)	Sepiolite Grade (%)	Enrichment Yield (%)
Raw Material	100	84	0
SP-01 AKM-40	88	88	92
SP-01 AKM-60	85	90	91
SP-01 AKM-80	76	92	82
SP-01 AKM-100	68	88	71
SP-01 AKM-140	33	66	26

As seen in Table 8, when the molar ratio is at 40%, the sepiolite grade increases to 88%, and the enrichment yield reaches 92%. When the molar ratio is 80%, the sepiolite grade increases to 92%, and the enrichment yield decreases to 82%. When the molar ratio exceeds 80%, the enrichment yield and the sepiolite grade decrease.

### 3.2. Flow curve measurements

With flow curve measurements, it was tried to define the changes in the flow curve of sepiolite suspensions evaluated under different operating parameters of the rotor-stator homogenizer. Flow curve experiments are important to understand the rheological behavior of sepiolite suspensions.

Flow curve studies using a linear scale for the shear rate axis may partially underestimate behavior in industrial applications with shear rates of  $10^0 \text{ s}^{-1}$  or below.

In industrial applications, the mechanical effects to which a dispersion or suspension is subjected at a shear rate below  $10^0 \text{ s}^{-1}$  are much more numerous and much longer than those to which it is subjected at shear rates above  $10^0 \text{ s}^{-1}$ . Therefore, in such studies, performing the analyses on a logarithmic scale rather than a linear scale provides more accurate, meaningful, and comparable results.

At this stage, flow curve measurements were performed using 24000, 18000, and 12000 rpm rotor speeds and 15.95, 11.96, and 7.98 m/s peripheral speeds. The relevant graphs are shown in Figs. 4, 5, and 6.

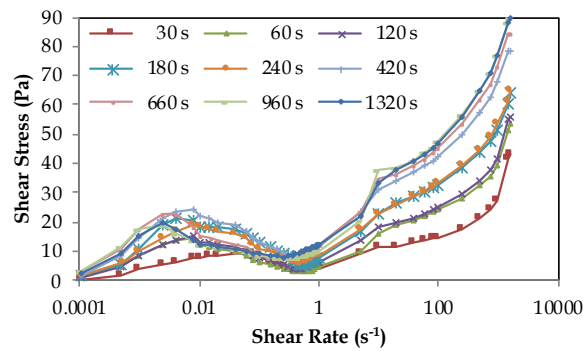


Fig. 4. Effects of mechanical activation time on the flow curve at 24000-rpm rotor speed and 15.95 m/s peripheral speed

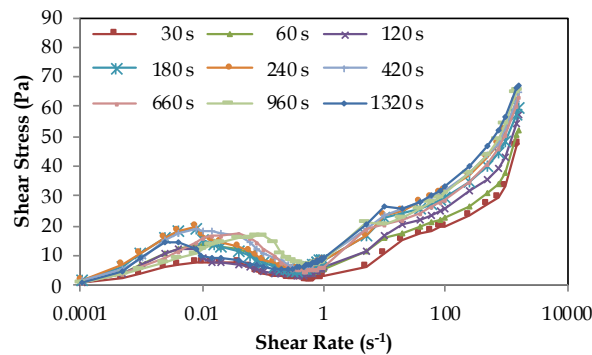


Fig. 5. Effects of mechanical activation time on the flow curve at 18000-rpm rotor speed and 11.96 m/s peripheral speed

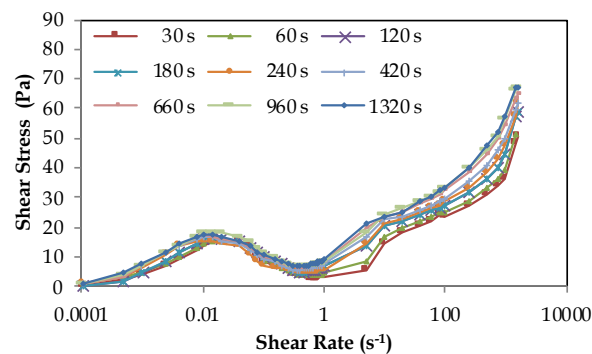


Fig. 6. Effects of mechanical activation time on the flow curve at 12000-rpm rotor speed and 7.98 m/s peripheral speed

When Fig. 4, 5, and 6 are evaluated,

- The increase in the shear stress observed in the shear speed range of  $10^0$  and  $10^3$   $s^{-1}$  at 24000 rpm, 15.95 m/s peripheral speed, 420, 660, 960, and 1320 s activation times was not observed in the measurements made at the same mechanical activation time with 11.96 m/s peripheral speed. It is thought that the main reason for this may be the insufficient amount of kinetic energy transferred to the suspension and the shear forces formed in the rotor-stator spray region.
- At 18000 rpm, 11.96 m/s peripheral speed, as the mechanical activation time increases, there is an increase in shear stress in the sliding speed range of  $10^0$  to  $10^3$   $s^{-1}$ , although not as much as at the rotor peripheral speed of 15.95 m/s. In the sliding speed range of  $10^{-4}$  to  $10^0$   $s^{-1}$ , there is a gradual increase and then a gradual decrease.
- At 12000 rpm, 7.98 m/s peripheral speed, as the mechanical activation time increases, there is an increase in the shear stress in the shear speed range of  $10^0$ - $10^3$   $s^{-1}$ . Unlike the rotor peripheral speed measurements of 15.95 m/s and 11.96 m/s, a continuous and gradual increase is observed in the shear stress between  $10^{-4}$  and  $10^0$   $s^{-1}$ .

According to Newton's laws, every object moves towards the lowest energy level when in motion. In suspensions, the increase in shear rate first causes the particles to move away from each other, and with the increase in shear rate, they orient and align towards the axis where they will encounter the least resistance in the flow axis. In flow curve measurements, it is thought that in the shear rate range of  $10^{-4}$  to  $10^{-2}$   $s^{-1}$ , the first separation of the particles from each other causes an increase in shear stress; when the shear rate increases from  $10^{-2}$  to  $10^0$   $s^{-1}$ , the particles move towards the lowest energy level, causing a decrease in shear stress; when the shear rate increases further and reaches the range of  $10^0$  to  $10^4$   $s^{-1}$ , the sepiolite fibers begin to form a stable network (matrix) and the shear stress increases again. This sequence of events is interpreted by taking inspiration from Newton's law of inertia.

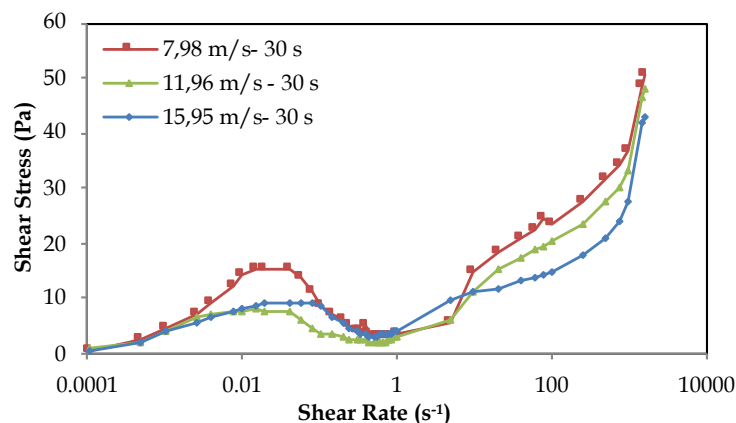


Fig. 7. Effects of 30-second mechanical activation time and peripheral speed on the flow curve

As seen in Fig. 7, as the rotor speed and indirectly the rotor peripheral speed increase, there is an increase in the shear stress in the  $10^0$  to  $10^3$   $s^{-1}$  shear speed range. As the shear speed approaches  $10^3$   $s^{-1}$ , the shear stresses approach each other. A change independent of the rotor peripheral speed is observed in the  $10^{-4}$ - $10^0$   $s^{-1}$  shear speed range. This phenomenon can be thought to be because the applied mechanical activation time is insufficient for the entire suspension to pass through the rotor-stator homogenizer head. For this reason, the sepiolite fibres cannot be activated homogeneously.

Figs. 8 and 9 show no marginal difference in the shear stress curves at 60 and 120 seconds of activation time, although the rotor and peripheral speeds indirectly increase.

After the 180-second activation time, the increase in rotor speed and, indirectly, the peripheral speed started to be effective again (Fig. 10). The measurement instabilities observed before this period were thought to be due to the lack of sufficient circulation in the suspension and, indirectly, the lack of homogeneous kinetic energy transfer.

Starting from the activation time of 420 seconds, the increase in rotor speed and indirectly the rotor peripheral speed began to affect the flow curves clearly (Fig. 12). It is thought that homogeneous circulation and kinetic energy transfer in the suspension occurred after this stage.

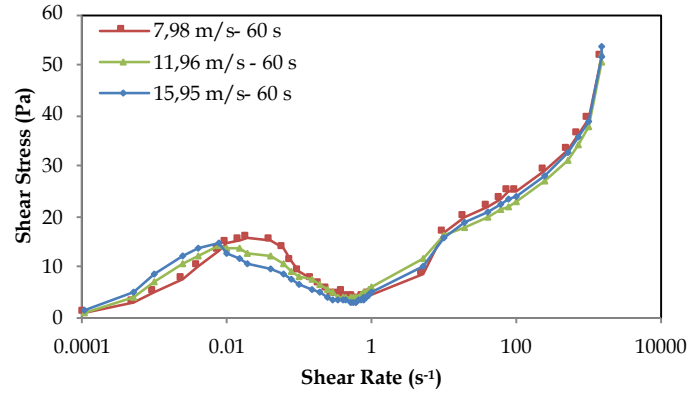


Fig. 8. Effects of 60-second mechanical activation time and peripheral speed on the flow curve

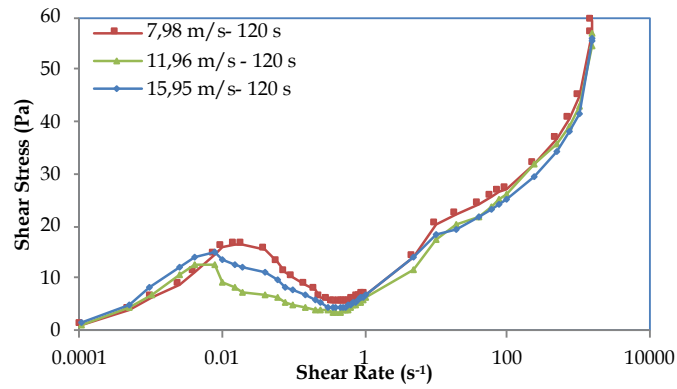


Fig. 9. Effects of 120-second mechanical activation time and peripheral speed on the flow curve

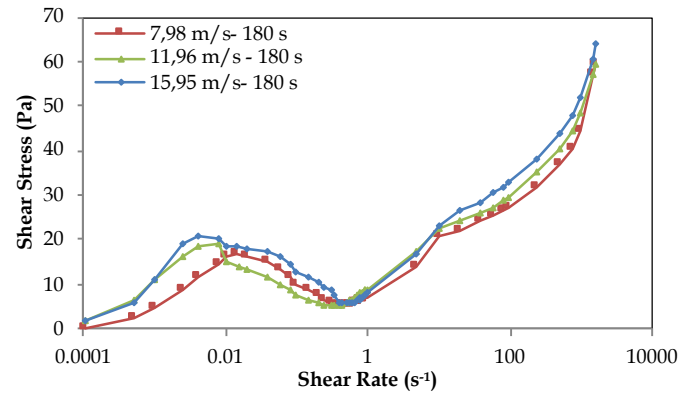


Fig. 10. Effects of 180-second mechanical activation time and peripheral speed on the flow curve

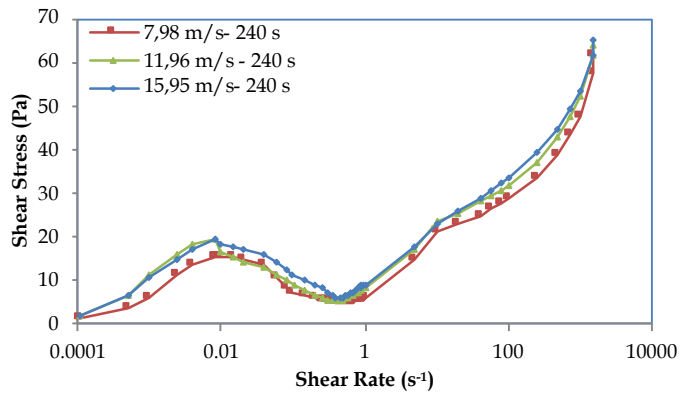


Fig. 11. Effects of 240-second mechanical activation time and peripheral speed on the flow curve

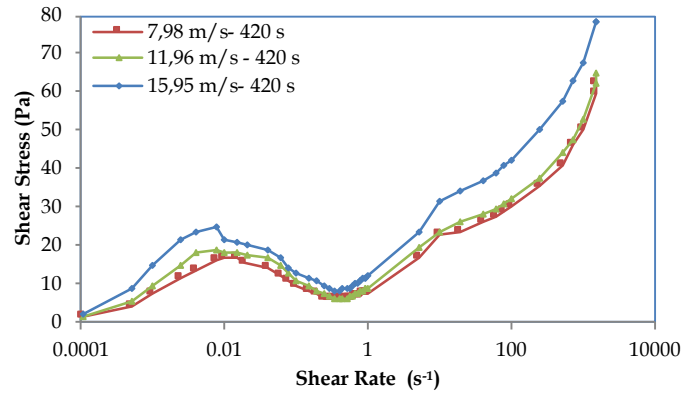


Fig. 12 Effects of 420-second mechanical activation time and peripheral speed on the flow curve

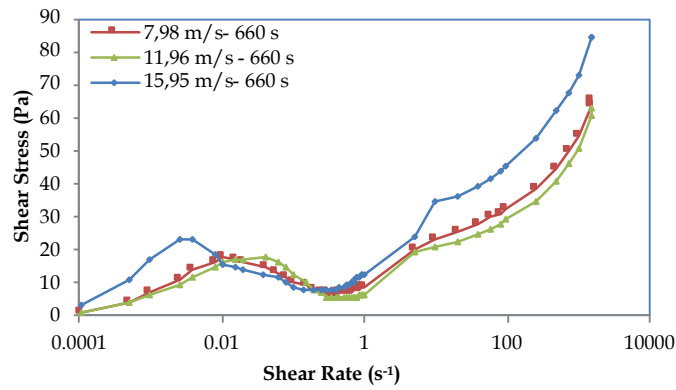


Fig. 13. Effects of 660-second mechanical activation time and peripheral speed on the flow curve

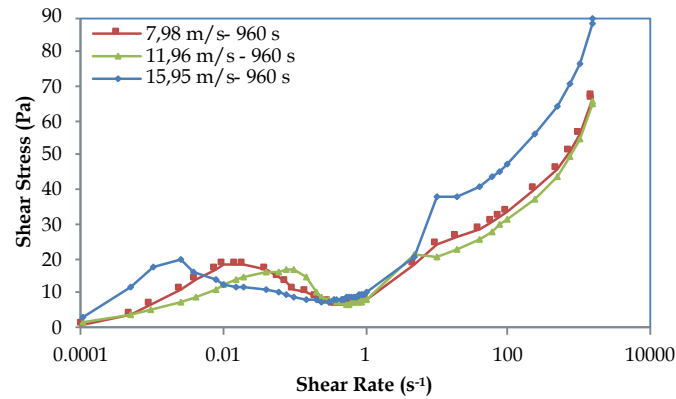


Fig. 14. Effects of 960-second mechanical activation time and peripheral speed on the flow curve

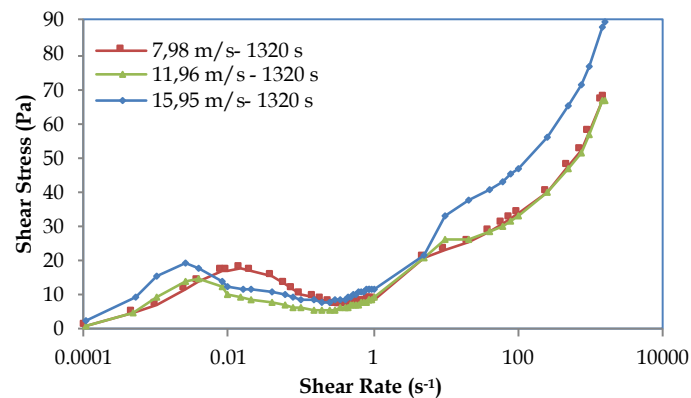


Fig. 15. Effects of 1320-second mechanical activation time and peripheral speed on the flow curve

As seen in Figs. 13, 14, and 15, the rotor speed and the rotor peripheral speed gave very close values for the measurements of 7.98 m/s and 11.96 m/s. On the other hand, an increase was observed in the measurements of 15.95 m/s.

Measurements were also made with different rotor head designs to investigate the effects of design and mechanical activation parameters on the flow curves.

In the measurements, the rotor peripheral speeds and rotor speed ratios were calculated and brought to equal values, and the effects of changes in mechanical activation and design parameters on the suspension's rheological behavior were examined using rotor-stator units of different designs at equal rotor peripheral speeds. Table 9, Figs. 16, 17, and 18 show the variations in mechanical activation characteristics when the peripheral speed remains constant in different rotor designs.

As seen in Table 9, the changes in the flow curve of the experiments where the peripheral speed (7.98 m/s) was kept constant and different rotor head designs were used are shown in Figs. 16, 17, and 18, respectively.

As seen in Figs. 16, 17, and 18, as the nominal shear force increases in the mechanical activation time of 120 seconds in the range of  $10^{-4}$  and  $10^3$  cutting speeds, the shear stress also increases. In the 420 and 660-second measurements, the shear stress difference between the nominal shear force of  $15958 \text{ s}^{-1}$  and

Table 9. Mechanical activation parameters of different rotor-stator designs at equal peripheral speed

Rotor speed rpm	Rotor peripheral speed m/s	Nominal shear force ( $N_{sr}$ ) $\text{s}^{-1}$	Kinetic energy transfer per unit volume ( $E_{\text{rotor}/\text{volume}}$ ) (J/s)/liter	Rotor blade-stator hole interaction number ( $N_{\text{interactions}}$ )
6500	7,98	6149	70,0	7800
7900	7,98	15958	46,9	2633
12000	7,98	39878	20,3	14400

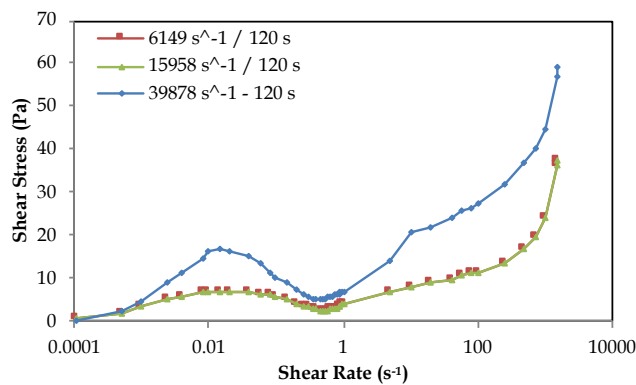


Fig. 16. Flow curve change after 120 seconds of mechanical activation at different rotor-stator designs and nominal cutting speeds

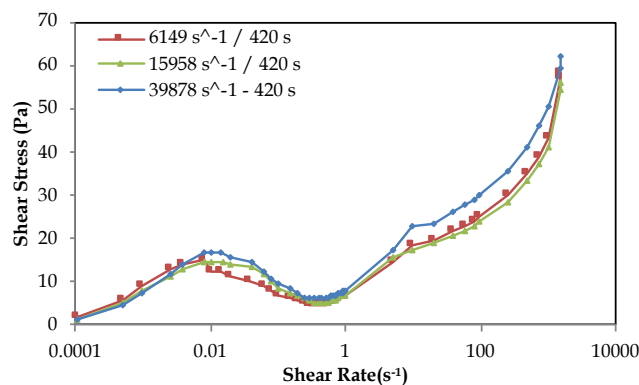


Fig.17. Flow curve change after 420 seconds of mechanical activation at different rotor-stator designs and nominal cutting speeds

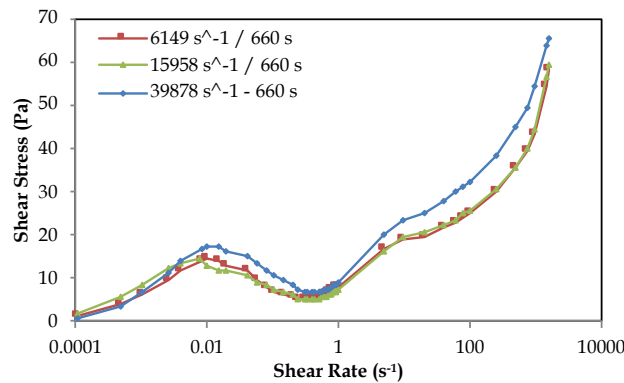


Fig. 18. Flow curve change after 660 seconds of mechanical activation at different rotor-stator designs and nominal cutting speeds

the nominal shear force of  $6149 \text{ s}^{-1}$  gradually decreases and becomes equal. On the other hand, the suspension subjected to mechanical activation under the nominal shear force of  $39878 \text{ s}^{-1}$  gives higher shear stress. Here, it can be said that the shear stress increases as the nominal shear forces increase, but this effect decreases as the activation time increases.

#### 4. Conclusions

The study revealed several important findings regarding mechanical activation and acid treatment of sepiolite. The key findings are:

- The optimal nitric acid concentration was found to be at an 80% molar ratio, increasing sepiolite content from 84.4% to 91.9%
- Increased acid concentrations resulted in the degradation of the sepiolite structure and a reduction in solid recovery
- At 24000 rpm (15.95 m/s peripheral speed), significant increases in shear stress were observed in the  $10^0$ - $10^3 \text{ s}^{-1}$  shear rate range
- Lower peripheral speeds (11.96 and 7.98 m/s) showed more gradual changes in rheological behaviour
- It was observed that mechanical activation times of at least 420 s were required for stable rheological properties and proper suspension circulation.
- At equal peripheral speeds, various rotor head designs had different effects on rheological properties.
- Higher nominal shear forces raised shear stress, while longer activation durations reduced this effect.
- Suspension behaviour is greatly affected by the interaction between design parameters and activation time.
- A minimum activation duration of 180 seconds is necessary for stable rheological behaviour.
- Rotor peripheral speed became increasingly influential after 420 seconds of activation
- The combination of high peripheral speed (15.95 m/s) and extended activation time (>660 seconds) produced the most stable rheological properties

These results have important consequences for improving sepiolite-processing conditions, especially in industrial uses demanding certain rheological properties. The work shows that obtaining appropriate sepiolite properties requires careful management of mechanical activation factors and acid treatment conditions.

#### Acknowledgments

The authors wish to acknowledge Akmin Mining Company for supplying the study samples.

#### References

- ALVAREZ, A., 1984. *Sepiolite: Properties and uses, Developments in sedimentology*. A. Singer ve E. Galan, Elsevier, 37, 253-287.

- ATIEMO-OBENG, A. V., CALABRESE, R. V., 2004. *Rotor-stator mixing devices*. E. L. Paul, V. A. Atiemo-Obengve S. M. Kresta, John Wiley & Sons, Inc.: Hoboken, NJ, 479-505.
- CAMPELO, J. M., GARCIA, A., LUNA, S., MARINAS, J. M., 1987. *Catalytic activity of natural sepiolites in cyclohexene skeletal isomerization*. *Clay Minerals* 22(2), 233-236.
- CORNEJO, J., & HERMOSIN, M. C., 1988. *Structural alteration of sepiolite by dry grinding*. *Clay Minerals*, 23(4), 391-398.
- ÇAĞLAR, U., 2019. *Enrichment of sepiolite by wet grinding and acid leaching methods and modelling of its rheological behavior*. Institute of Science, ESOĞU, PhD Thesis.
- ÇINAR, M., 2005. *Sepiyolitın reolojik özelliklerinin belirlenmesi ve su bazlı sepiyolit üretimi*. Fen Bilimleri Enstitüsü, İTÜ, Doktora Tezi.
- ÇINAR, M., CAN, M. F., SABAH, E., KARAGÜZEL, C., ÇELİK, M. S., 2009. *Rheological properties of sepiolite ground in acid and alkaline media*. *Applied Clay Science* 42(3), 422-426.
- DÉKÁNY, I., TURI, L., FONSECA, A., NAGY, J. B., 1999. *The structure of acid treated sepiolites: Small-angle x-ray scattering and multi mas-nmr investigations*. *Applied Clay Science* 14(1), 141-160.
- DE LIMA, J. A., CAMILO, F. F., FAEZ, R., & CRUZ, S. A., 2017. *A new approach to sepiolite dispersion by treatment with ionic liquids*. *Applied Clay Science*, 143, 234-240.
- FRANCO, F., POZO, M., CECILIA, J. A., BENÍTEZ-GUERRERO, M., POZO, M., VD., 2014. *Microwave assisted acid treatment of sepiolite: The role of composition and "crystallinity"*. *Applied Clay Science* 102, 15 – 27.
- GALAN, E., 1996. *Properties and applications of palygorskite-sepiolite clays*. *Clay Minerals*, 31(4), 443-453.
- JIMÉNEZ-LÓPEZ, A., LÓPEZ-GONZÁLEZ, J. D. D., RAMÍREZ-SÁENZ, A., RODRÍGUEZ-REINOSO, F., VALENZUELA-CALAHORRO, C., VD., 1978. *Evolution of surface area in a sepiolite as a function of acid and heat treatments*. *Clay Minerals* 13(4), 375-385.
- MYERS, K. J., REEDER, M. F., RYAN, D., DALY, G., 1999. *Get a fix on high-shear mixing*. *Chemical engineering progress* 95(11), 33-42.
- MYRIAM, M., SU, M., M. MART, J., 1998. *Structural and textural modifications of palygorskite and sepiolite under acid treatment*.
- ÖZDEMİR, M., & KIPÇAK, İ., 2004. *Dissolution kinetics of sepiolite in hydrochloric acid and nitric acid*. *International Journal of Mineral Processing*, 75(1-2), 91-99.
- RODRIGUEZ, M. V., GONZALEZ, J. D. D. L., MUNOZ, M. B., 1994. *Acid activation of a spanish sepiolite: Physico-chemical characterization, free silica content and surface area of products obtained*. *Clay Minerals* 29(3), 361- 367.
- SABAH, E., & ÇELİK, M. S., 1998. *Sepiyolit: Özellikleri ve Kullanım Alanları*. 3. Endüstriyel Hammaddeler Sempozyumu, İzmir, Turkey.
- SANTAREN, J., 1993. *Sepiolite: A mineral thickener and rheology additive*. *Modern Paint and Coatings* 98, 72.
- SIMONTON, T. C., KOMARNENI, S., ROY, R., 1988. *Gelling properties of sepiolite versus montmorillonite*. *Applied Clay Science* 3(2), 165-176.
- SUÁREZ, M., & GARCÍA-ROMERO, E., 2012. *Variability of the surface properties of sepiolite*. *Applied Clay Science*, 67, 72-82.
- TOMURA, S., INUKAI, K., MIYAWAKI, R., 1995. *Purification of sepiolite and palygorskite*. *Journal of the Society of Materials Engineering for Resources of Japan* 8(1), 90-98.
- VUČELIĆ, D., SIMIĆ, D. S., KOVAČEVIĆ, O., DOJČINOVIĆ, M. M., MITROVIĆ, M., 2002. *The effects of grinding on the physicochemical characteristics of white sepiolite from golesh*. *Journal of the Serbian Chemical Society* 67(3), 197-211.
- XU, J., ZHANG, J., WANG, Q., WANG, A., 2011. *Disaggregation of palygorskite crystal bundles via high-pressure homogenization*.
- ZHENG, Y. P., ZHANG, J. X., LAN, L., & YU, P. Y., 2011. *Sepiolite nanofluids with liquid-like behavior*. *Applied Surface Science*, 257(14), 6171-6174.